Diffusion coefficients of fluorescent organic molecules in inert gases

ARTICLE *in* APPLIED PHYSICS LETTERS · JULY 2013

Impact Factor: 3.3 · DOI: 10.1063/1.4816960

2 AUTHORS, INCLUDING:

Cedric Rolin
imec Belgium
21 PUBLICATIONS **443** CITATIONS

AIP | Applied Physics Letters

Diffusion coefficients of fluorescent organic molecules in inert gases

Cedric Rolin and Stephen R. Forrest

Citation: Appl. Phys. Lett. **103**, 041911 (2013); doi: 10.1063/1.4816960
View online: http://dx.doi.org/10.1063/1.4816960
View Table of Contents: http://apl.aip.org/resource/1/APPLAB/v103/i4
Published by the AIP Publishing LLC.

Diffusion coefficients of fluorescent organic molecules in inert gases

Cedric Rolin and Stephen R. Forrest[a)]
Departments of Electrical Engineering and Computer Science, Physics, and Materials Science and Engineering, University of Michigan, Ann Arbor, Michigan 48109, USA

(Received 16 June 2013; accepted 13 July 2013; published online 25 July 2013)

We use arrested-flow pulse broadening to measure the diffusion coefficients of four archetype organic semiconductors in two carrier gases, N_2 and Ar, with a precision of 5%. The measurements are realized by the injection and transport of pulses of organic molecules in an organic vapor phase deposition chamber, followed by their detection using laser induced fluorescence that dynamically measures the organic concentration in the gas phase. Measurements show that the diffusivity of *tris*(8-hydroxyquinoline) aluminum (Alq_3) in N_2 and Ar varies as the square of the temperature and inversely with pressure over a large range of gas conditions. We show that classical Chapman-Enskog theory can be used to approximate the diffusivity with an accuracy that depends on the physical dimensions of the organic molecular species, with the most accurate predictions for spherical and rigid molecules such as Alq_3. © *2013 AIP Publishing LLC*.
[http://dx.doi.org/10.1063/1.4816960]

The diffusion kinetics of small organic molecules in inert gases governs several processing techniques that rely on a carrier gas to transport the molecules from their evaporation source to the point of condensation. Such techniques include physical vapor transport for the growth of single crystals,[1] organic vapor-liquid-solid growth,[2] organic vapor phase deposition[3] (OVPD) of thin films, and vapor jet printing of micron-scale patterns.[4] In these cases, carrier gas flow is typically laminar with a low Reynolds number, and transport of the organic species is both convective and diffusive.[5–8] Convection speeds up mass transport, increases the purity of the condensate, and allows for flexibility in system design. On the other hand, carrier gas boundary layers formed in the vicinity of instrument walls and substrate result in diffusion-limited transport in these regions.[6–10] A precise understanding of diffusion, therefore, is required to control and optimize mass transport, leading to a desired film or crystal morphology. This understanding starts with the evaluation of the diffusivity of the organic vapor in its carrier gas.

A number of techniques exist to measure gas diffusion coefficients,[11] although none can be used at the elevated temperatures and low pressures characteristic of the vapor-phase methods employed in organic growth. This has led to estimations of the molecular diffusivities in an inert gas carrier obtained by extrapolating existing theories to a variety of material systems and process conditions.[5,7,10,12] In this work, we directly and precisely measure the diffusion coefficients of four archetype organic molecular species in N_2 or Ar by means of the arrested-flow pulse broadening method.[13] The experiments are carried out within an OVPD reactor equipped with a laser induced fluorescence (LIF) capability to measure the time-resolved *in situ* concentration of organic molecules in the vapor.[14] From this method, we obtain the diffusivity as a function of temperature and pressure. We also provide a theoretical framework to understand the results and to predict the diffusivities of other molecular systems.

The diffusion coefficient, D_{12}, of a low density binary gas mixture of species 1 and 2 is given to first approximation by Chapman-Enskog theory, that is,[11,15,16]

$$D_{12} = \frac{3k_BT}{8P\sigma_{12}^2\Omega_{12}(T)}\sqrt{\frac{N_Ak_BT}{2\pi}\left(\frac{1}{m_1}+\frac{1}{m_2}\right)}. \quad (1)$$

Here, k_B is Boltzmann's constant, N_A is Avogadro's constant, T and P are the temperature and pressure, m_α is the molecular mass of species α, σ_{12} is the collision diameter of the pair of molecules, and Ω_{12}(T) is the collision integral for diffusion that accounts for the deviation from elastic collisions between rigid spheres due to intermolecular forces. Using the Lennard-Jones 6-12 intermolecular potential to estimate these forces, the values of Ω_{12}(T) have been tabulated as a function of the dimensionless temperature k_BT/ε_{12}, where ε_{12} is the maximum attractive energy between the pair of molecules.[15,17] Also, σ_{12} and ε_{12} are parameters of the Lennard-Jones potential, viz.: $\sigma_{12} = \frac{\sigma_1+\sigma_2}{2}$ and $\varepsilon_{12} = \sqrt{\varepsilon_1\varepsilon_2}$. Here, σ_α is the molecular diameter of species α, and ε_α is the intermolecular energy of attraction of the pure gas, α.[18] Using a corresponding states principle, $\varepsilon_\alpha/k_B = 1.92\,T_m$, where T_m is the melting point of the pure substance.[15] Since the collision integral, Ω_{12}(T), decreases with T, then[19]

$$D_{12} = D_{12,0}\frac{T^n}{P}, \quad (2)$$

where $D_{12,0}$ is a constant, and the exponent $1.5 < n < 2.0$ is a function of T and the material system.[11]

Material pulse broadening techniques are often employed in gas chromatography to measure diffusion coefficients of a solute vapor in a carrier gas.[19,20] That is, D_{12} is extracted from analysis of the broadening of short impulses of material travelling down the chromatographic column. An accurate measurement requires the isolation of the effects of diffusion from other instrumental broadening phenomena. This can be

a)E-mail: stevefor@umich.edu

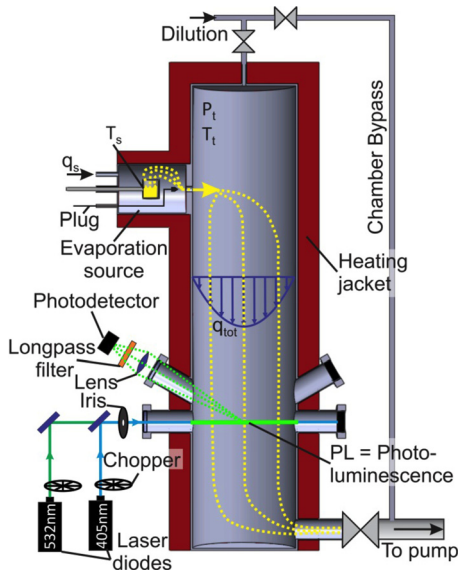

FIG. 1. Schematic of an OVPD reactor with a laser-induced fluorescence (LIF) capability to dynamically measure organic species concentration in the gas phase. Here, q_s and q_{tot} are the mass flow rates of carrier gas injected in the source and the tube respectively, T_s and T_t are the source and tube temperatures, P_t is the tube pressure, and PL is the photoluminescence.

achieved by the arrested-flow method:[13] Once the pulse has reached mid-column height, the carrier gas flow is stopped for a duration, t_a, during which the pulse broadens only by diffusion. Carrier gas flow is then restarted to collect and measure the pulse height and width. This process is repeated for several different arrest times, t_a. The pulse width, σ^2, linearly increases with t_a, following:[13]

$$\frac{d\sigma^2}{dt_a} = 2\frac{D_{12}}{\bar{u}_{cg}^2}, \tag{3}$$

where $\bar{u}_{cg}$ is the average carrier gas velocity, obtained from a measurement of the arrival times of molecules in a long saturated pulse.[14]

The diffusivity of organic molecules in a hot inert carrier gas has been measured in the OVPD system[21] illustrated in Fig. 1. The system consists of a uniformly heated tube ($T_t \approx 340\,^\circ$C) pumped to a typical pressure of $P_t = 1.5$ Torr. Radial temperature measurements indicate that the gas temperature is in equilibrium with the walls across the tube cross-section. In the source barrel, the organic material powder is contained in an alumina crucible heated to T_s. The source plug valve and the flow of carrier gas (N_2 or Ar) in the source (with a typical flow rate of $q_s = 100$ sccm) were timed to inject 3 s square pulses of organic molecular vapor into the main tube. Four organic materials were tested: tris(8-hydroxy-quinolinato)aluminium (Alq_3) ($T_s = 300\,^\circ$C); 9,10-di(naphth-2-yl)anthracene (ADN) ($T_s = 270\,^\circ$C); boron subphthalocyanine chloride (SubPc) ($T_s = 310\,^\circ$C); and rubrene ($T_s = 265\,^\circ$C). Upon injection, the organic vapor was further diluted with carrier gas in the main tube, giving a total carrier gas flow of $q_{tot} = 200$ sccm.

The organic vapor concentration was dynamically monitored close to the tube outlet by means of LIF, described previously.[14] In LIF, output from a diode laser (at a wavelength of 405 nm for Alq_3 and ADN, 532 nm for SubPc and rubrene) excites the organic molecules in the gas phase. These molecules subsequently fluoresce as measured by a photodetector angled towards the center of excitation beam. The fluorescence intensity is a linear function of the molecular concentration in the gas.

For arrested flow measurements, the OVPD tube was equipped with valves and an auxiliary bypass tube (see Fig. 1) that interrupt the flow in the main tube without a significant perturbation of the pressure. Six seconds following the injection of an organic vapor pulse into the main OVPD tube, the pulse travel was stopped for a time t_a by switching total carrier gas flow q_{tot} to the bypass line. Then, switching the carrier gas flow back to the main tube restarted pulse travel and enabled the organic species concentration measurement using LIF.

Figure 2(a) shows a series of concentration profiles measured by LIF, corresponding to pulses of Alq_3 in an Ar carrier for arrest times, t_a, varied from 0 to 40 s. The detection time of each peak follows the 5 s increments in t_a. As the organic vapor diffuses, the pulse height decreases and the width

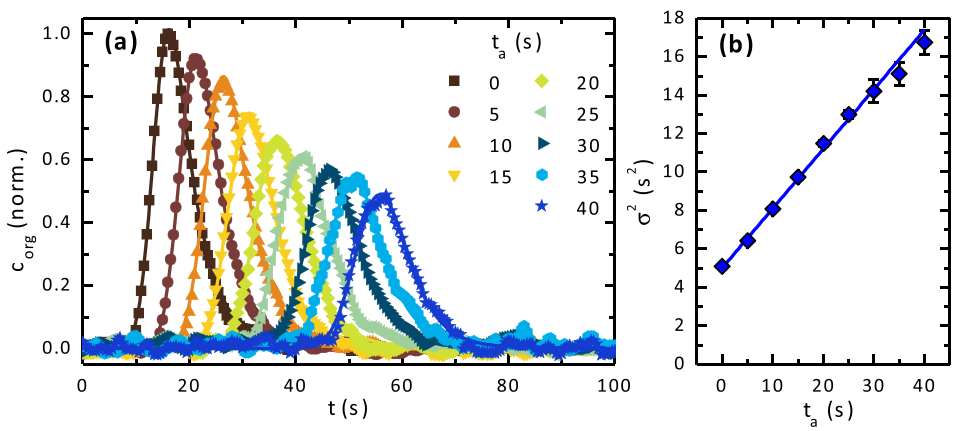

FIG. 2. (a) Concentration of Alq_3 as a function of time, t, for a series of organic material pulses into the OVPD reactor and transported by Ar. The pulses are shown for several arrest times, t_a. All pulses are generated with the following conditions: Source temperature $T_s = 300\,^\circ$C, source carrier gas mass flow rate $q_s = 100$ sccm, tube pressure $P_t = 1.5$ Torr, total carrier gas mass flow rate $q_{tot} = 200$ sccm, and tube temperature $T_t = 340\,^\circ$C. All pulses are generated by a 3 s long injection from the organic material source. Following 6 s after injection, the travel of each pulse is arrested for a time, t_a, by switching all carrier gas flow to the bypass line. The solid lines are fits by the EMG function with a fixed $\tau = 4.6$ s for all pulses. (b) Evolution of the pulse width, σ^2, with arrest time, t_a, obtained from the EMG fits in (a). The solid line is a linear fit.

TABLE I. Diffusion coefficients of Alq_3, ADN, SubPc, and rubrene in N_2 and Ar measured experimentally and calculated using the Chapman-Enskog theory. T_t and P_t are the tube temperature and pressure, respectively.

	$D_{org\text{-}N_2}$ (cm^2/s)			$D_{org\text{-}Ar}$ (cm^2/s)				
Molecule	Exp.	Theor.	Dev. (%)	Exp.	Theor.	Dev. (%)	T_t (°C)	P_t (Torr)
Alq_3	28.0 ± 2.2	28.2	0.6	23.7 ± 1.2	23.5	−0.8	340	1.5
ADN	25.5 ± 3.6	22.5	−11.6	21.5 ± 2.2	18.7	−13.1	300	1
SubPc	18.5 ± 2.5	27.5	48.9	15.9 ± 2.8	23.0	44.7	340	1.5
Rubrene	13.0 ± 2.4	20.5	58.0	11.0 ± 2.5	17.1	55.1	280	1.5

broadens. The asymmetry of the pulses in Fig. 2(a) is caused by material retention during material transit from source to measurement location.[14] To account for this phenomenon, the pulses are fit to an exponential modified Gaussian (EMG) function that convolutes a Gaussian distribution (with variance σ^2) with an exponential decay (with characteristic time, τ). The exponential decay includes retention effects, which are constant for all pulses. The fit based on EMG, therefore, requires a single, constant τ that is equal to the value of the fit for the pulse at $t_a = 0$ s. The fit to each transient yields σ^2, which is plotted vs. t_a in Fig. 2(b). The evolution of σ^2 with t_a is linear with a slope $d\sigma^2/dt_a = 0.28 \pm 0.01$ s.

In addition to the series of short pulses, a 60 s long pulse is generated under the same carrier gas flow conditions. From fits to this latter transient,[14] we obtain an average carrier gas velocity of $\bar{u}_{cg} = 13.0 \pm 0.1$ cm/s. Using these fitted values in Eq. (3) gives $D_{Alq_3\text{-}Ar} = 23.7 \pm 1.2$ cm^2/s for Alq_3 in Ar at $T_t = 340$ °C and $P_t = 1.5$ Torr. The precision of the measurement of D_{12} is set by the error estimates for $d\sigma^2/dt_a$ and $\bar{u}_{cg}$, which vary between 5% and 20% in our experimental series. Similar experiments were conducted to measure the diffusivities of the four organic compounds in N_2 and Ar, with results summarized in Table I along with the corresponding measurement conditions.

Table I also shows D_{12} calculated using the Chapman-Enskog theory in Eq. (1). The Lennard-Jones parameters used are provided in Table II. For each organic compound, the attractive energy, ε_α/k, is estimated from the melting point T_m, and the molecular diameter σ_α is approximated as the equal to the diameter of the smallest sphere enclosing the relaxed molecular geometries. These geometries were optimized through a quantum chemical computation using the density functional B3LYP method with a 6_31G basis set, taking into account the van der Waals radii of each atom. To quantify the anisotropy of the optimized molecular shape, we calculated the fractional anisotropy of each compound via

$$FA = \sqrt{\frac{(\lambda_1 - \lambda_2)^2 + (\lambda_2 - \lambda_3)^2 + (\lambda_3 - \lambda_1)^2}{2(\lambda_1^2 + \lambda_2^2 + \lambda_3^2)}}, \quad (4)$$

where $\lambda_{1,2,3}$ are the three radii of the smallest ellipsoid enclosing the molecule. Here, $FA = 0$ for a sphere, and $FA \rightarrow 1$ when the largest radius tends to infinity. The values of FA given in Table II show that Alq_3 is closest to spherical, whereas ADN is the most anisotropic molecule. Finally, the computations provide the magnitude of the molecular dipole moments, p, also listed in Table II.

Measurements of $D_{Alq_3-N_2}$ and $D_{Alq_3\text{-}Ar}$ vs. T_t and P_t are shown in Figs. 3(a) and 3(b), respectively. The theoretical values for $D_{Alq_3\text{-}N_2}$ (solid line) and $D_{Alq_3\text{-}Ar}$ (dashed line) calculated with Eq. (1) are also shown. The Chapman-Enskog theory matches the measured values over the entire experimental range investigated. Moreover, by fitting Eq. (2) to the data, we observe that both $D_{Alq_3\text{-}N_2}$ and $D_{Alq_3\text{-}Ar}$ increase with $T_t^{1.9 \pm 0.1}$ and are inversely proportional to P_t.

From Table I, we find that the diffusion coefficients of the organic species are ~20% higher in N_2 than in Ar. This difference originates from the reduced mass term, $m_1^{-1} + m_2^{-1}$, in Eq. (1), which is primarily determined by the lighter carrier gas. The effect of the carrier gas on the Lennard-Jones parameters, σ_{12} and ε_{12}, is less important, as these are dominated by the larger and more strongly bound organic species. In consequence, a lighter carrier gas such as He is expected to increase the diffusivity of the organic species by ~150% compared with N_2.

The agreement between experiment and theory in Fig. 3 is not as good for molecules other than Alq_3 (see Table I). The theory underestimates D_{12} for ADN, while it overestimates this value for SubPc and rubrene. One source of these discrepancies lies in inaccuracies in determining the collision integral, $\Omega_{12}(T)$. This parameter is calculated by assuming the elastic scattering of molecules whose intermolecular forces are described by a spherical potential that is only valid for non-polar molecules. The large, non-spherical organic molecules studied here have many internal rotational and vibrational degrees of freedom, enabling energy exchange during inelastic collisions. Non-sphericity also leads to inaccuracies in estimating collision diameters, scattering angles, and the maximum attractive energy ε_{12} used in the spherical Lennard-Jones potential. Finally, two of the molecules possess a non-negligible permanent dipole moment (see Table II), which can lead to departures in the estimation of intermolecular forces.

While many of these complications have been previously addressed for simpler gas systems,[11,16,18] the molecules studied here have irregular shapes and physical properties, making the determination of collision integrals $\Omega_{12}(T)$ a considerable challenge. Molecular dynamics simulations may offer a suitable means for their theoretical

TABLE II. Molecular properties used to parameterize the Chapman-Enskog theory. m is the molecular mass, T_m is the melting point, ε_α/k_B and σ_α are the maximum intermolecular attractive energy and the molecular diameter of species α, FA is the fractional anisotropy of the molecular shape, and p is the magnitude of the molecular dipole.

Molecule	m (AMU)	T_m (°C)	ε_α/k_B (K)	σ_α (Å)	FA	p (D)
N_2	28	…	99.8[a]	3.67[a]	…	0
Ar	40	…	122.4[a]	3.43[a]	…	0
Alq_3	459	416	1323	14.9[b]	0.17[b]	4.954[b]
ADN	431	383	1259	20.3	0.39	0.051
SubPc	431	360	1215	15.3	0.21	5.646
Rubrene	533	331	1160	16.3	0.23	0.002

[a]From Ref. 15.
[b]Values computed for the meridional isomer of Alq_3.

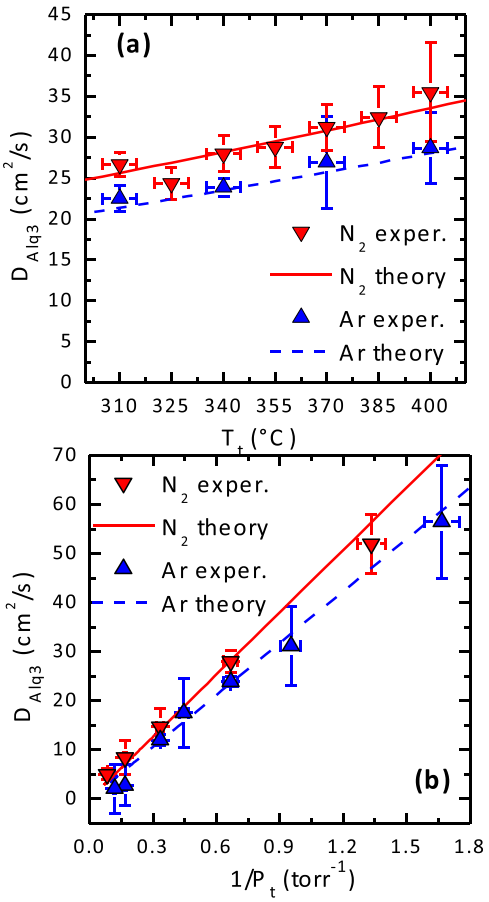

FIG. 3. Diffusion coefficients of Alq_3 in N_2 and Ar as functions of (a) tube temperature, T_t, with a tube pressure of $P_t = 1.5$ Torr and (b) as a function of the inverse of P_t with a $T_t = 340\,°C$. The lines are theoretical diffusivities, calculated using the Chapman-Enskog theory.

understanding,[22] although this is beyond the scope of this work. Nevertheless, the Chapman-Enskog theory accurately predicts the diffusion coefficients of Alq_3. The fit is simplified due to the near spherical shape of the molecule, validating the use of a Lennard-Jones potential. Indeed, while the fits are not as accurate for the other less spherically symmetric molecules, Chapman-Enskog theory is able to provide useful estimates of diffusion coefficients for such molecules.

In conclusion, we have used arrested-flow pulse broadening to measure the diffusion coefficients of four archetype organic semiconductors (Alq_3, ADN, SubPc, and rubrene) in two carrier gases, N_2 and Ar, with a precision of 5%. This method was implemented by the injection and transport of pulses of organic molecules in an organic vapor phase deposition chamber, followed by their detection using laser-induced fluorescence that dynamically measures the organic concentration in the gas phase. Measurements carried out under different gas flow conditions show that the diffusivity of Alq_3 in N_2 and Ar varies as $T^{1.9}$ and $1/P$ over the range of gas conditions employed. Values of the diffusion coefficient are also calculated using the Chapman-Enskog theory with a collision integral based on a Lennard-Jones intermolecular potential. This simple model offers a first approximation of the diffusion coefficients, with greater accuracy found for rigid and spherical molecules such as Alq_3. The measurements and theory are useful for the quantitative prediction of the mass transport of organic molecules in a carrier gas at high temperatures and low pressures. This has potential applications in several applications relying on the use of a carrier gas for the transport and deposition of organic molecular materials.

We thank Dr. Olga Lobanova Griffith for her help with the quantum chemical computations. We are grateful to the SunShot Program of the US Department of Energy (EERE) under award number DE-EE0005310 (CR, experiment, analysis) and Universal Display Corp. (CR, LIF) for partial financial support of this work. This work was also supported by the U.S. Department of Energy (DOE), Office of Basic Energy Sciences, as part of the Center for Energy Nanoscience, Energy Frontier Research Center, Grant #DE-SC0001013 (SRF, analysis).

[1]R. Laudise, C. Kloc, P. Simpkins, and T. Siegrist, J. Cryst. Growth **187**, 449 (1998).
[2]D. W. Shaw, K. Bufkin, A. A. Baronov, B. L. Johnson, and D. L. Patrick, J. Appl. Phys. **111**, 074907 (2012).
[3]M. Baldo, M. Deutsch, P. Burrows, H. Gossenberger, M. Gerstenberg, V. Ban, and S. R. Forrest, Adv. Mater. **10**, 1505 (1998).
[4]M. Shtein, P. Peumans, J. B. Benziger, and S. R. Forrest, Adv. Mater. **16**, 1615 (2004).
[5]M. Shtein, P. Peumans, J. B. Benziger, and S. R. Forrest, J. Appl. Phys. **93**, 4005 (2003).
[6]M. Shtein, H. F. Gossenberger, J. B. Benziger, and S. R. Forrest, J. Appl. Phys. **89**, 1470 (2001).
[7]G. J. McGraw and S. R. Forrest, J. Appl. Phys. **111**, 043501 (2012).
[8]C. Rolin, *Vapor Phase Deposition of Organic Semiconductors: Application to Field Effect Transistors* (LAP Lambert Academic Publishing, Saarbrücken, Germany, 2010).
[9]M. Heuken and N. Meyer, in *Organic Electronics: Materials, Manufacturing, and Applications*, edited by H. Klauk (Wiley-VCH, Weinheim, Germany, 2006), pp. 203–232.
[10]M. Shtein, in *Organic Electronics: Materials, Processing, Devices and Applications*, edited by F. So (CRC, Boca Raton, FL, USA, 2009), pp. 27–57.
[11]T. R. Marrero and E. A. Mason, J. Phys. Chem. Ref. Data **1**, 3 (1972).
[12]C. Rolin, K. Vasseur, J. Genoe, and P. Heremans, Org. Electron. **11**, 100 (2010).
[13]J. Knox and L. McLaren, Anal. Chem. **36**, 1477 (1964).
[14]C. Rolin, G. Vartanian, and S. R. Forrest, J. Appl. Phys. **112**, 113502 (2012).
[15]R. B. Bird, W. E. Stewart, and E. N. Lightfoot, *Transport Phenomena* (Wiley, New York, USA, 2007).
[16]S. Chapman, *The Mathematical Theory of Non-Uniform Gases*, 3rd ed. (Cambridge University, New-York, USA, 1990).
[17]J. O. Hirschfelder, R. B. Bird, and E. L. Spotz, J. Chem. Phys. **16**, 968 (1948).
[18]J. O. Hirschfelder, R. B. Bird, and E. L. Spotz, Chem. Rev. **44**, 205 (1949).
[19]G. Karaiskakis, in *Encyclopedia of Chromatography*, 2nd ed., edited by J. Cazes (Taylor & Francis, Boca Raton, FL, USA, 2005), pp. 459–467.
[20]G. Karaiskakis and D. Gavril, J. Chromatogr. A **1037**, 147 (2004).
[21]R. R. Lunt, B. E. Lassiter, J. B. Benziger, and S. R. Forrest, Appl. Phys. Lett. **95**, 233305 (2009).
[22]K. Chae, P. Elvati, and A. Violi, J. Phys. Chem. B **115**, 500 (2011).